JACS
JOURNAL OF THE AMERICAN CHEMICAL SOCIETY
Article
pubs.acs.org/JACS

Sustainable Synthesis of Zeolites without Addition of Both Organotemplates and Solvents

Qinming Wu,[†] Xiong Wang,[†] Guodong Qi,[§] Qiang Guo,[‡] Shuxiang Pan,[†] Xiangju Meng,*[,†] Jun Xu,[§] Feng Deng,[§] Fengtao Fan,[‡] Zhaochi Feng,[‡] Can Li,*[,‡] Stefan Maurer,[#] Ulrich Müller,[#] and Feng-Shou Xiao*[,†]

[†]Department of Chemistry, Key Lab of Applied Chemistry of Zhejiang Province, Zhejiang University, Hangzhou, 310007, P. R. China
[§]State Key Laboratory of Magnetic Resonance and Atomic and Molecular Physics, Wuhan Center for Magnetic Resonance, Wuhan Institute of Physics and Mathematics, Chinese Academy of Sciences, Wuhan, 430071, P. R. China
[‡]State Key Laboratory of Catalysis, Dalian Institute of Chemical Physics, Chinese Academy of Sciences, Dalian, 116023, P. R. China
[#]Process Research and Chemical Engineering, BASF SE, 67056, Ludwigshafen, Germany

Supporting Information

ABSTRACT: The development of sustainable and environmentally friendly techniques for synthesizing zeolites has attracted much attention, as the use of organic templates and solvents in the hydrothermal synthesis of zeolites is a major obstacle for realizing green and sustainable synthesis ways. Recently, the introduction of the organotemplate-free synthesis method allowed avoiding the use of organic templates, but water as solvent was still required; solvent-free routes on the other hand beared the potential to significantly reduce the amount of polluted wastewater, but organic templates were still present. In this work, we have demonstrated a combined strategy of both organotemplate- and solvent-free conditions to synthesize aluminosilicate zeolites Beta and ZSM-5 (S-Beta and S-ZSM-5), two of the most important zeolites relevant for industry. The samples are thoroughly characterized by XRD patterns, SEM images, N_2 sorption isotherms, UV-Raman spectra, and ^{29}Si and ^{27}Al MAS NMR spectra. The results demonstrate that S-Beta and S-ZSM-5 zeolites exhibit almost the same textural parameters (e.g., BET surface area and pore volume) and catalytic performance in cumene cracking and *m*-xylene isomerization as those of conventional Beta and ZSM-5 zeolites synthesized under hydrothermal conditions (C-Beta and C-ZSM-5). The organotemplate- and solvent-free syntheses of S-Beta and S-ZSM-5 take place at a low-pressure regime and are free of harmful gases as well as give high product yields together with highly efficient consumption of the starting raw materials. These advantages plus the very simple procedures opened the pathway to a highly sustainable zeolite synthesis protocol compared to conventional methods currently employed for C-Beta and C-ZSM-5. Very interestingly, this simple synthesis is a good model for understanding zeolite crystallization. The detail characterizations indicate that the S-Beta crystals are formed from the assembly of zeolite building units, mainly 4MRs, while the 5MRs in the framework are just formed in the crystallization of S-ZSM-5, rather than existence in the starting solid mixture. During the crystallization processes, small traces of water play an important role for the hydrolysis and condensation of silica and/or aluminosilicate species.

1. INTRODUCTION

Zeolites, especially aluminosilicate zeolites, have been widely used as catalysts in the industrial processes of oil refining and production of fine chemicals due to their high surface area, large pore volume, uniform microporous channels, and excellently thermal and hydrothermal stabilities.[1−29] In general, zeolites are made in a so-called solvothermal synthesis in the presence of toxic and costly organic templates and large amounts of solvents such as water and/or alcohols, often in sealed autoclaves under autogenous pressure.[30,31] The use of expensive organic templates not only increases the zeolite cost but also results in the production of harmful gases for removing the organic templates by combustion at high temperature.[1−37] The presence of solvents in the solvothermal synthesis is to ensure efficient transport of reactants, but the solvents occupy a large space in autoclaves, which strongly influence the product yield.[1−37] In addition, high autogenous pressure and polluted wastes from the solvents also results in safety and environmental concerns.[1−37]

Recently, to overcome the drawbacks brought from using toxic and costly organic templates, an organotemplate-free synthesis route was successfully developed based on a seed-directed route for synthesizing aluminosilicate zeolites, where the zeolite crystals are grown from the induction of zeolite seeds in the absence of any organic templates.[38−64] Later, this synthesis has been quickly scaled up by BASF (Ludwigshafen, Germany).[39]

Received: January 6, 2014
Published: February 19, 2014

dx.doi.org/10.1021/ja500098j | J. Am. Chem. Soc. 2014, 136, 4019−4025

However, this methodology normally gives relatiely low zeolite yield, which is due to the use of a large amount of water solvent.[38−64]

In the previous works, great efforts were made for increasing zeolite product yields and reducing autogenous pressure as well as reduction of polluted residues in the synthesis.[32,65−67] In 1990, Xu et al. reported synthesis of zeolites from dry gel conversion or vapor phase transport technique.[65] Later, Matsukata and co-workers designed a similar steam-assisted conversion to prepare zeolites.[66] Schüth and co-workers have reported hydrothermal zeolite syntheses from "dry" starting materials.[67] These syntheses significantly increase zeolite product yield but still require the presence of organic templates. In addition, Morris et al. have developed an ionothermal synthesis route for synthesizing zeolites, where the safety concerns are completely eliminated due to very low vapor pressure of the ionic liquids.[32] Notably, the ionic liquids in the synthesis served as both solvents and organic templates.

More recently, Ren et al. and Jin et al. reported solvent-free synthesis of aluminosilicate and aluminophosphate-based zeolites with advantages of increasing zeolite yield and eliminating high-pressure conditions.[68,69] Morris et al. highlighted the importance of the solventless synthesis and pointed out that the combination of solventless synthesis and organo-template-free routes should be the ultimate goal for synthesizing zeolites on an environmental sustainable basis. A particularly interesting candidate might be the BEA* structure as it was demonstrated that Beta can be prepared without the use of organic SDA, and furthermore Beta is known as an excellent catalyst for many industrial relevant processes.[70]

In this work, we report a novel strategy for synthesizing BEA* and MFI zeolite structures by combination of organotemplate- and solvent-free routes. The synthetic processes and the zeolite properties were carefully investigated. The zeolites synthesized show comparable textural parameters and catalytic performance to conventional zeolites synthesized under hydrothermal conditions.

2. EXPERIMENTAL SECTION

Materials. Aluminum sulfate [$Al_2(SO_4)_3{\cdot}18H_2O$, AR, 99%, Sinopharm Chemical Reagent Co., Ltd.], sodium hydroxide (NaOH, AR, 96%, Sinopharm Chemical Reagent Co., Ltd.), $Na_2SiO_3{\cdot}9H_2O$ (SiO_2 of 20 wt.%, Tianjin Guangfu Chemical Reagent Co, Ltd.), solid silica gel (Qingdao Haiyang Chemical Reagent Co, Ltd.), $NaAlO_2$ (Sinopharm Chemical Reagent Co, Ltd.), $SiO_2{\cdot}3H_2O$ (homemade), and ammonium nitrate (NH_4NO_3, AR, 99%, Beijing Chemical Reagent Co., Ltd.) were used without further purification.

Synthesis. As a typical run for the synthesis of Beta zeolite without addition of water as solvent, 6.34 g of $SiO_2{\cdot}3H_2O$ (hydrated form of solid silica gel), 0.73 g of $NaAlO_2$, 0.48 g of NaOH, and 0.34 g of calcined Beta seeds (Si/Al = 12.5) were added together. After grinding for 10−20 min, the powder mixture was transferred to an autoclave and sealed. After heating at 120 °C for 9 days, the sample was completely crystallized (designated as S-Beta), giving 3.0 g product. The H-form of the sample was prepared by ion exchange with 1 M NH_4NO_3 solution and calcination at 500 °C for 4 h. The ion-exchange procedure was repeated once.

As a typical run for the synthesis of ZSM-5 zeolite without addition of water as solvent, 1.5 g of $NaSiO_3{\cdot}9H_2O$ (SiO_2, 20wt.%), 0.65 g of $Al_2(SO_4)_3{\cdot}18H_2O$, 1.35 g of solid silica gel, and 0.17 g of calcined ZSM-5 (Si/Al = 150) seeds were added together. After grinding for 10−20 min, the powder mixture was transferred to an autoclave and sealed. After heating at 180 °C for 13 h, the sample was completely crystallized (designated as S-ZSM-5), giving 1.9 g product. The H-form of the sample was prepared from ion exchange with 1 M NH_4NO_3 solution and calcination at 500 °C for 4 h. The ion exchange was repeated once.

Characterization. X-ray powder diffraction (XRD) patterns were measured with a Rigaku Ultimate VI X-ray diffractometer (40 kV, 40 mA) using CuK_α (λ=1.5406 Å) radiation. The N_2 sorption isotherms at the temperature of liquid nitrogen were measured using Micromeritics ASAP 2020 M and Tristar system. The sample composition was determined by inductively coupled plasma (ICP) with a Perkin-Elmer 3300DV emission spectrometer. Scanning electron microscopy (SEM) experiments were performed on Hitachi SU-1510 electron microscopes. UV Raman spectra were measured with a Jobin-Yvon T64000 triple-stage spectrometer with spectral resolution of 2 cm^{-1}. The laser line at 325 nm of a He/Cd laser was used as an exciting source with an output of 50 mW. The power of the laser at the sample was ~3.0 mW. ^{27}Al and ^{29}Si MAS NMR spectra were recorded on a Bruker AVANCE^{III} 500WB spectrometer. Single-pulse ^{27}Al MAS spectra were acquired using a 4 mm probe with a short radio frequency (rf) pulse of 0.25 μs (corresponding to a $\pi/15$ flip angle), a pulse delay of 1.0 s, and a spinning rate of 12 kHz. Single-pulse ^{29}Si MAS NMR experiments with ^1H decoupling were performed using a 7 mm probe with a $\pi/4$ pulse width of 4.0 μs, a 60 s pulse delay, and a spinning rate of 4 kHz.

Catalytic tests. Cumene cracking was performed at 300 °C by pulse injections. In each run, 50 mg of catalyst was used, the pulse injection of the reactant was 0.4 μL, and the reaction flow rate was 55 mL/min.

Catalytic *m*-xylene isomerization to *p*-xylene was carried out in a fixed-bed reactor. The zeolite sample (200 mg, 20−40 mesh) was first activated in dry air at 450 °C for 2 h and then cooled to reaction temperature (350 °C) in a flow of dry nitrogen. *m*-Xylene was fed (WHSV = 3 h^{-1}) by a metering pump, vaporized in a preheated assembly, and then passed through the catalyst. The product was analyzed by online gas chromatography (GC1690) with FID detector using HP-FFAP column.

3. RESULTS AND DISCUSSION

Synthesis of Beta Zeolite. Figure 1 shows XRD pattern, SEM image, N_2 sorption isotherms, and ^{29}Si MAS NMR spectrum of Beta zeolite synthesized without addition of both organotemplate and water (S-Beta). The XRD pattern shows a series of characteristic peaks associated with BEA structure (Figure 1a). The SEM image exhibits almost perfect crystals (Figure 1b), confirming relatively high crystallinity. The N_2 sorption isotherms displays typical Langmuir-type curve (Figure 1c). Typical for microporous materials a steep increase at low

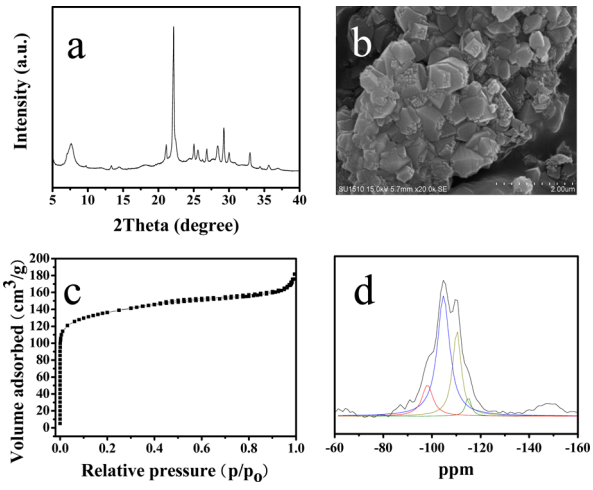

Figure 1. (a) XRD pattern, (b) SEM image, (c) N_2 sorption isotherms, and (d) ^{29}Si NMR spectrum of S-Beta sample. The measurement of the N_2 sorption isotherms is from the H-form and the other measurements from as-synthesized S-Beta sample.

dx.doi.org/10.1021/ja500098j | J. Am. Chem. Soc. 2014, 136, 4019−4025

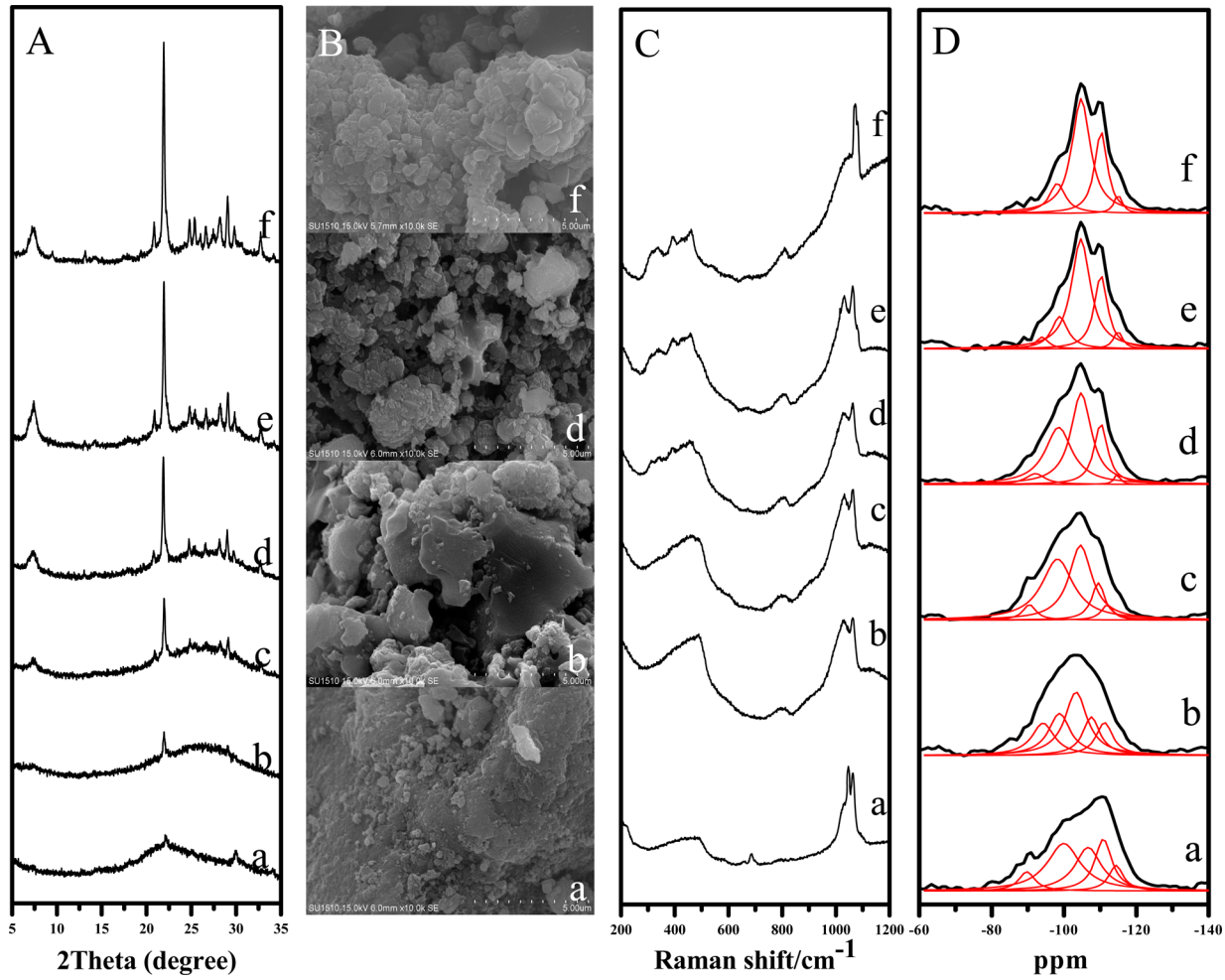

Figure 2. (A) XRD patterns, (B) SEM images, (C) UV-Raman spectra, (D) ^{29}Si NMR spectra of S-Beta samples crystallized at (a) 0, (b) 2, (c) 4, (d) 5, (e) 7, and (f) 9 days, respectively.

relative pressure $10^{-6} < P/P_0 < 0.01$, due to the filling of micropores by N_2 is observed. Correspondingly, the sample BET surface area and micropore volume are 464 m^2/g and 0.21 cm^3/g, respectively, in good agreement with those (445 m^2/g and 0.21 cm^3/g) of Beta zeolite synthesized in the presence of water under hydrothermal conditions (C-Beta, Figure S1). The ^{29}Si NMR spectrum (Figure 1d) exhibits peaks at about −115.0, −110.3, −104.7, and −98.2 ppm. The peaks at −115 and −110.3 ppm are assigned to Si(4Si) species; the peak at −104.7 ppm is assigned to Si(3Si,1Al) and/or Si(3Si,1OH); the peak at −98.2 ppm is assigned to Si(2Si,2Al), Si(2Si,1Al,1OH), and/or Si(2Si,2OH). ICP analysis shows that Si/Al ratio in the product is ∼5.9.

Notably, Beta seeds play an important role in the synthesis. If Beta seeds are absent in the solid starting mixtures, the obtained products are always amorphous or MOR zeolite (Run 1 in Table S1). After addition of Beta seeds to the starting mixtures, S-Beta zeolites with good crystallinity are obtained (Run 2 and 3 in Table S1). In addition, it is found that the ratios of SiO_2/Na_2O and SiO_2/Al_2O_3 also strongly influence the synthesis of S-Beta zeolite. When the SiO_2/Na_2O ratio is lower than 4.52, the product contains GIS and MOR impurity (Run 4, Table S1). When the SiO_2/Na_2O ratio is higher than 5.67, the product comprises MOR impurity (Run 5, Table S1). When the SiO_2/Al_2O_3 ratio is 12, the product contains GIS and MOR impurity (Run 6, Table S1). When the SiO_2/Al_2O_3 is 17, S-Beta zeolite is obtained (Run 2, Table S1). Therefore, the SiO_2/Na_2O ratios at 4.72−5.12 and the SiO_2/Al_2O_3 ratios close to 17 are suitable for synthesis of S-Beta.

To get a better understanding of the synthesis, the crystallization process of S-Beta has been intensively investigated by XRD, SEM, UV-Raman, and NMR techniques, as shown in Figure 2 and Figure S2. The photographs of the samples crystallized at various time in a closed glass tube (Figure S3) show that the samples are always in a solid phase during the crystallization process, indicating full solid conversion. Before crystallization, the sample shows very weak peaks associated with Beta seeds (Figure 2A-a), which are related to the Beta seeds existing in the starting mixtures. After crystallization for 2 days, the sample displays stronger peaks associated with BEA zeolite (Figure 2A-b). At the same time, small amounts of crystalline products were visible via SEM (Figure 2B-b). Increasing the crystallization time from 4 to 7 days, the XRD peaks gradually grow in intensity (Figure 2A-c-e). Correspondingly, more S-Beta zeolite crystals were observed in the isolated solid (Figure 2B-d). When the crystallization time reaches 9 days, S-Beta with high crystallinity can be obtained (Figure 2A-f and B-f). The dependence of S-Beta crystallinity on crystallization time is shown in Figure S4.

Figure 2C shows UV-Raman spectra recorded for S-Beta samples crystallized at various time. The initial aluminosilicate solid mixture shows a major broad band at 493 cm^{-1} associated with four-membered rings of T−O−T (4MRs). In addition, the

dx.doi.org/10.1021/ja500098j | J. Am. Chem. Soc. 2014, 136, 4019−4025

aluminosilicate solid mixture in the absence of Beta seeds also shows a broad band at 493 cm^{-1} (Figure S5), suggesting that this band should result from the solid mixture, rather than the Beta seeds. Notably, the band at 493 cm^{-1} in Figure 2C-a gradually shifted to lower wavenumber (485 cm^{-1}), which is attributed to the rearrangement and self-assembly of zeolite building units, mainly 4MRs. After crystallization for 4 days, UV-Raman spectrum gives weak band at 342 cm^{-1} associated with six-membered rings (6MRs), 396 cm^{-1} associated with five-membered rings (5MRs), and 431, 460, and 485 cm^{-1} associated with 4MRs.[71,72] By increasing the crystallization time to 9 days, the sample shows strong bands at 342, 396, 431, and 460 cm^{-1} associated with characteristic bands of Beta zeolites,[71,72] together with complete disappearance of the band at 485 cm^{-1}. This observation suggests that the formation of S-Beta zeolite mainly results from assembling zeolite building units at 485 cm^{-1}. Usually, it is well-known that 4MRs, 5MRs, and 6MRs are building units for construction of Beta zeolite structure.[71,72] However, as observed in UV-Raman spectra, the starting solid mixture predominantly consists of 4MRs, suggesting that 4MRs might be the active building units for crystallization of S-Beta zeolite, while 5MRs and 6MRs are just formed after the formation of the S-Beta zeolite framework.

Figures 2D and S2 show ^{29}Si and ^{27}Al NMR spectra of solid samples obtained from crystallization at various time (0−9 days). The structural information on S-Beta samples is presented in Tables S2 and S3. Before crystallization, the Si(2Si) species are dominant (intensity 36.1%, Figure 2D-a). After crystallization for 2 days, the Si(2Si) signal intensity is decreased to 21.5%, while the Si(3Si) signal intensity increases (33%) (Figure 2D-b). This phenomenon might be related to the rearrangement of zeolite building units. At the same time, a broad signal in the range of 50−70 ppm is observed in the ^{27}Al NMR spectrum, mainly attributed to Al(3Si) and Al(4Si) species (Figure S2-b).[73] It is worth mentioning that the concentration of Si(2Si) species is increasing with the crystallization time from 2 to 4 days, while decreasing with the crystallization time from 4 to 9 days. The enrichment of Si(2Si) species should be assigned to the hydrolysis of silica species due to the presence of a little amount of water in the solid mixture, while the remarkable reduction of Si(2Si) species at elongated crystallization period could be attributed to the crystallization of zeolites by condensation of Si(2Si) species containing hydroxyl groups. After crystallization for 9 days, the ^{29}Si NMR spectrum exhibits major peaks at −104.7 and −110.5 ppm associated with Si(3Si) and Si(4Si) species (Figure 2D-f). Simultaneously, the ^{27}Al spectrum shows a major peak at 57 ppm (Figure S2-f), corresponding to tetrahedral coordination of framework Al. These results are consistent with those of Beta zeolite synthesized under hydrothermal conditions.[42]

From our observation we suggest that S-Beta crystals are formed from the assembly of zeolite building units, which mainly consist of 4MRs. During this process, the hydrolysis and condensation of silica species occur, suggesting an important role of a little amount of water in the synthesis.

Synthesis of ZSM-5 Zeolite. Figure 3 shows XRD pattern, SEM image, N_2 sorption isotherms, and ^{29}Si MAS NMR spectrum of ZSM-5 zeolite synthesized without addition of both organotemplate and water (S-ZSM-5). The XRD pattern gives a series of characteristic peaks associated with MFI structure (Figure 3a). The SEM image shows typical MFI crystal morphology (Figure 3b). Figure 3c shows N_2 sorption isotherms, giving a Langmuir-type curve. Typical for microporous materials

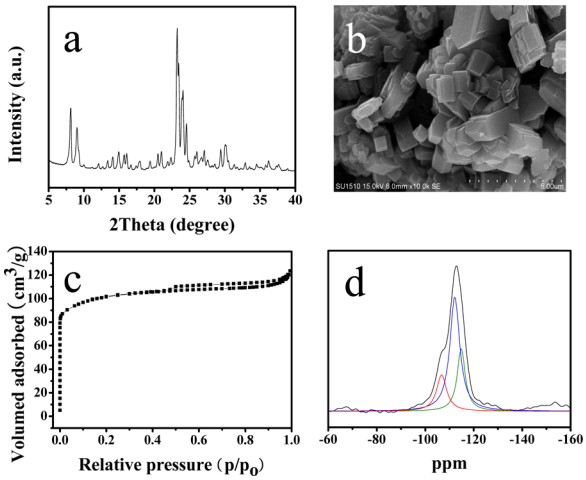

Figure 3. (a) XRD pattern, (b) SEM image, (c) N_2 sorption isotherms, and (d) ^{29}Si NMR spectrum of S-ZSM-5 sample. N_2 sorption isotherm is obtained from the H-form, other measurements are as-synthesized S-ZSM-5 sample.

a steep increase at low relative pressure $10^{-6} < P/P_0 < 0.01$, due to the filling of micropores by N_2 is observed. The sample BET surface area and micropore volume are 345 m^2/g and 0.16 cm^3/g, which is comparable with those (350 m^2/g and 0.16 cm^3/g) of conventional MFI zeolite (Figure S6). The ^{29}Si NMR spectrum (Figure 3d) shows signals at −114.8, −112.2, and −106.7 ppm. The peaks at −114.8 and −112.2 ppm are assigned to Si(4Si) species; the peak at −106.7 ppm is assigned to Si(3Si,1Al) and/or Si(3Si,1OH). ICP analysis shows that Si/Al ratio of S-ZSM-5 is about 13. In the synthesis of S-ZSM-5, the use of ZSM-5 seeds and adjusting SiO_2/Al_2O_3 ratios is very important. When the ZSM-5 seeds are absent in the synthesis, the obtained solids are always amorphous materials (Run 1, Table S4); when ZSM-5 seeds are present, perfect ZSM-5 crystals could be obtained (Run 2, Table S4). These results confirm the importance of ZSM-5 seeds for synthesizing S-ZSM-5 zeolite. In addition, when the ratio of SiO_2/Al_2O_3 in the synthesis is 20, the product exhibits MOR impurity (Run 3, Table S4); when the SiO_2/Al_2O_3 ratio reaches to 40, the product contains an impurity of dense phase (Run 4, Table S4). Therefore, the suitable SiO_2/Al_2O_3 ratio is found at about 28.5. Notably, when totally anhydrous reagents (such as fumed silica) are used or ambient pressure is performed, we cannot synthesize S-ZSM-5 zeolite owing to the shortage of a few water in the synthesis system. These results confirm the importance of a few water in the synthesis. The minimum amount of water required for the synthesis of S-ZSM-5 zeolite with good crystallinity is a H_2O/SiO_2 ratio of at least 1.0. Interestingly, S-ZSM-5 product could be used as seeds to synthesize S-ZSM-5-2nd sample in the following run under the template-free and solvent-free conditions (Run 5, Table S4).

The crystallization of S-ZSM-5 has also been monitored with XRD, SEM, UV-Raman, and ^{29}Si and ^{27}Al NMR techniques (Figures 4 and S7). Similarly to BEA, the photographs of the samples crystallized at various time in a closed glass tube (Figure S8) show that the synthesis of S-ZSM-5 is a solid process. Before crystallization, the XRD pattern gives weak signals associated with ZSM-5 seeds (Figure 4A-a). After crystallization for 3 h, the intensity of the MFI related signals is lower (Figure 4A-b), indicating that the ZSM-5 seeds are partially dissolved in the alkaline solid mixture at 180 °C. After further elongation of the crystallization time to 5.5 h, the peaks associated with MFI

dx.doi.org/10.1021/ja500098j | J. Am. Chem. Soc. 2014, 136, 4019−4025

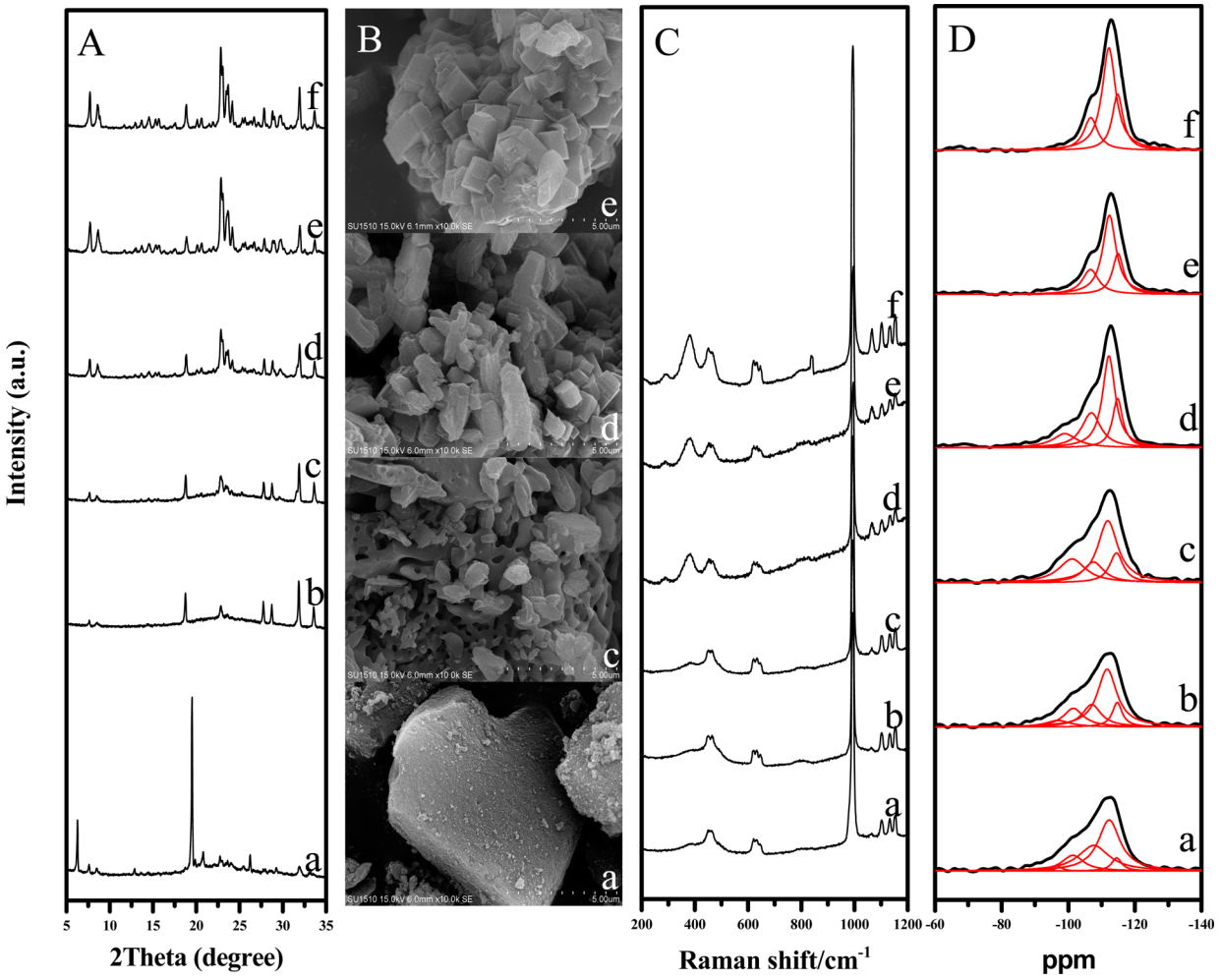

Figure 4. (A) XRD patterns, (B) SEM images, (C) UV-Raman spectra, (D) ^{29}Si NMR spectra of S-ZSM-5 samples crystallized at (a) 0, (b) 3, (c) 5.5, (d) 9, (e) 13, and (f) 17 h, respectively.

structure grow again (Figure 4A-c). At the same time, typical ZSM-5 crystals are visible in the SEM of the isolated products (Figure 4B-c). Increasing the crystallization time to 9 h, the intensity of XRD peaks gradually increases (Figure 4A-d). Correspondingly, more MFI zeolite crystals are formed (Figure 4B-d). When the crystallization time extends 13 h, no obvious change in crystallinity can be observed anymore (Figure 4A-f). The dependence of S-ZSM-5 crystallinity on crystallization time is displayed in Figure S9.

Figure 4C shows UV-Raman spectra recorded for S-ZSM-5 samples crystallized at various time. Before crystallization, the sample exhibits a very weak band at 380 cm^{-1} and strong bands at 455 and 995 cm^{-1}. The two strong bands are assigned to SO_4^{2-} species, while the very weak band should be assigned to 5MRs, which might result from the ZSM-5 seeds added to the solid mixture. In comparison, it does not observe any bands at near 380 cm^{-1} for the solid mixture in the absence of ZSM-5 seeds (Figure S10). After crystallization for 9 h, the sample exhibits strong band at 380 cm^{-1}, which is assigned to 5MRs in the framework. These results suggest that the 5MRs in the framework are mainly formed in the crystallization of S-ZSM-5. By increasing the crystallization time from 9 to 17 h, the sample UV-Raman spectra give higher band intensity, in agreement with increasing the sample crystallinity. These results confirm that the 5MRs are formed in the crystallization of S-ZSM-5.

Figures 4D and S6 show the ^{29}Si and ^{27}Al NMR spectra of S-ZSM-5 samples crystallized at various time (0−17 h). The structural information on S-ZSM-5 is presented in Tables S5 and S6. Before crystallization, Si(4Si) and Si(3Si) signals are dominant (52.4% and 32.1%). After crystallization for 3 h, the signal intensity of Si(3Si) species is significantly reduced (18.2%), probably due to hydrolysis of silica species in the presence of a little amount of water in the solid mixture. At the same time, the signal intensity of Si(4Si) species is slightly increased (59.2%) owing to condensation of silica species. Increasing the crystallization time from 3 to 9 h, the Si(4Si) signals gradually increase, which is assigned to crystallization of S-ZSM-5 zeolite. When the crystallization time extends 13 h, no obvious change in the intensity of the Si(4Si) signal can be observed, indicating that the crystallization of S-ZSM-5 zeolite is completed. The ^{27}Al NMR spectra for all the samples show a sharp signal centered near 55 ppm, indicating tetrahedral coordination of the Al species.

From the observations during the crystallization, it is difficult to find the building units of 5MRs in the starting solid materials except for the presence of a small amount of zeolite seeds, although MFI structure is rich in 5MRs. The 5MRs are just formed during crystallization of S-ZSM-5 zeolite, rather than being starting building units for the formation of S-ZSM-5. The important role of small amounts of water in the synthesis of S-

dx.doi.org/10.1021/ja500098j | J. Am. Chem. Soc. 2014, 136, 4019−4025

ZSM-5 can be observed in the change in Si(3Si) concentration, related to the hydrolysis and condensation of silica species during the course of the crystallization.

Catalytic Tests. Figure 5 shows the catalytic properties of S-Beta in cumene cracking, respectively, S-ZSM-5 in *m*-xylene

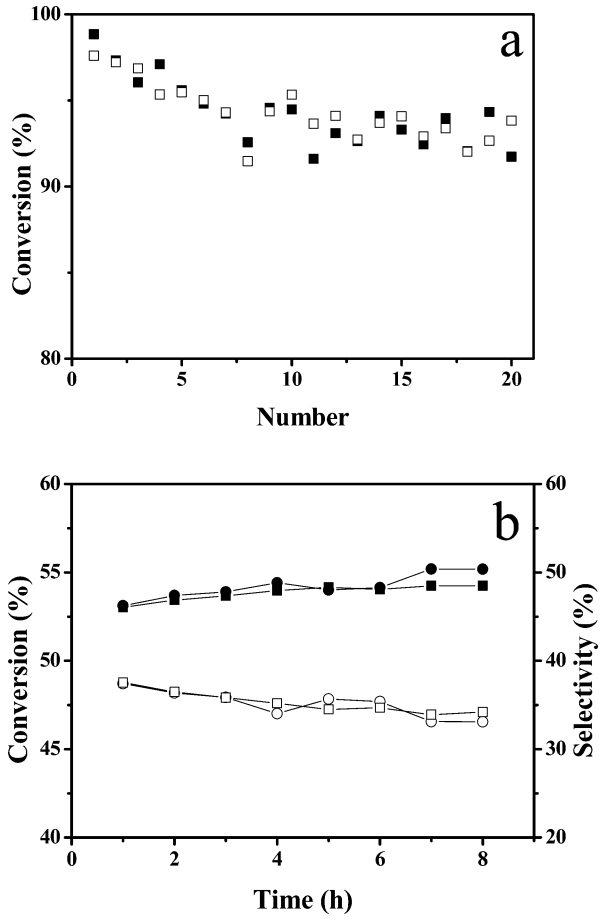

Figure 5. (a) Catalytic cumene cracking over S-Beta (□ conv.) and C-Beta (■ conv.) zeolites and (b) catalytic performance in *m*-xylene isomerization over S-ZSM-5 (□ conv.; ■ sel.) and C-ZSM-5 (○ conv.; ● sel.) zeolites as a function of number and time.

isomerization, which is found to be very comparable with those of conventional Beta and ZSM-5 zeolites. Notably, in both cumene cracking and *m*-xylene isomerization, S-Beta and S-ZSM-5 zeolites exhibit almost the same activity and selectivity as well as very similar catalyst life. These results indicate that S-Beta and S-ZSM-5 have comparable catalytic properties with conventional corresponding zeolites.

4. CONCLUSIONS

In summary, we have developed a novel synthesis route by combining the advantages of both organotemplate- and solvent-free synthesis conditions giving access to aluminosilicates such as zeolites Beta and ZSM-5 on a highly sustainable way exhibiting the following benefits: (1) Avoidance of using toxic and expensive organic templates, which significantly reduce zeolite costs and the environmental impact. (2) Avoidance of harmful gases formed by combustion of organic templates at high temperature, which not only gives savings in energy but also is ecologically beneficial. (3) High yields of zeolitic products, due to full utilization of the autoclave volume. In conventional hydrothermal synthesis, water occupies a large space of the autoclave volume. For example, when 3.68 g of SiO_2 sources was crystallized in 15 mL of an autoclave, it was obtained 3.0 g of S-Beta product. In contrast, when 0.83 g of SiO_2 source was crystallized in the same autoclave under conventionally hydrothermal conditions, it was obtained only 0.22 g of Beta-SDS product.[39] (4) A significant reduction of reaction pressure, achieved by both organotemplate- and solvent-free synthesis conditions, giving good safety concerns. (5) High efficiency for consumption of the starting raw materials, due to the removal of solvents for dissolution of partial nutrients in the synthesis. In addition, not consumed nutrients dissolved in the solvents and the conventional hydrothermal synthesis are added to the wastewater. (6) A simple and convenient procedure, which means to save energy and cost in the synthesis of zeolite. Considering these advantages, it is suggested that S-Beta and S-ZSM-5 can be named as sustainable obtained zeolites. Very importantly, the zeolites synthesized from the combined route of both organotemplate- and solvent-free route show almost the same textural parameters (BET surface area and pore volume) and catalytic properties in cumene cracking, respectively, *m*-xylene isomerization compared to conventional zeolites. The combination of sustainable zeolite synthesis with comparable properties allows to widely apply these S-Beta and S-ZSM-5 zeolites in industrial processes in the near future.

■ ASSOCIATED CONTENT

Ⓢ Supporting Information

Characterization details. This material is available free of charge via the Internet at http://pubs.acs.org.

■ AUTHOR INFORMATION

Corresponding Authors

mengxj@zju.edu.cn
canli@dicp.ac.cn
fsxiao@zju.edu.cn

Notes

The authors declare no competing financial interest.

■ ACKNOWLEDGMENTS

This work is supported by the Natural National Science Foundation of China (21273197, 21333009, and 21203165), National High-Tech Research and Development program of China (2013AA065301), BASF SE, and Fundamental Research Funds for the Central Universities (2013XZZX001).

■ REFERENCES

(1) Davis, M. E.; Lobo, R. F. *Chem. Mater.* **1992**, *4*, 756.
(2) Gies, H.; Marler, B. *Zeolite* **1992**, *12*, 42.
(3) Corma, A. *Chem. Rev.* **1995**, *95*, 559.
(4) Davis, M. E. *Nature* **2002**, *417*, 813.
(5) Cundy, C. S.; Cox, P. A. *Chem. Rev.* **2003**, *103*, 663.
(6) Ma, S. Q.; Sun, D. F.; Wang, X. S.; Zhou, H. C. *Angew. Chem., Int. Ed.* **2007**, *46*, 2458.
(7) Moliner, M.; Gonzalez, J.; Portilla, M. T.; Willhammar, T.; Rey, F.; Llopis, F. J.; Zou, X. D.; Corma, A. *J. Am. Chem. Soc.* **2011**, *133*, 9497.
(8) Chen, H. Y.; Wydra, J.; Zhang, X. Y.; Lee, P. S.; Wang, Z. P.; Fan, W.; Tsapatsis, M. *J. Am. Chem. Soc.* **2011**, *133*, 12390.
(9) Liu, F. J.; Willhammar, T.; Wang, L.; Zhu, L. F.; Sun, Q.; Meng, X. J.; Carrillo-Cabrera, W.; Zou, X. D.; Xiao, F. S. *J. Am. Chem. Soc.* **2012**, *134*, 4557.
(10) Zhang, X. Y.; Liu, D. X.; Xu, D. D.; Asahina, S.; Cychosz, K. A.; Agrawal, K. V.; Al Wahedi, Y.; Bhan, A.; Al Hashimi, S.; Terasaki, O.; Thommes, M.; Tsapatsis, M. *Science* **2012**, *336*, 1684.

(11) Lee, P. S.; Zhang, X. Y.; Stoeger, J. A.; Malek, A.; Fan, W.; Kumar, S.; Yoo, W. C.; Al Hashimi, S.; Penn, R. L.; Stein, A.; Tsapatsis, M. *J. Am. Chem. Soc.* **2011**, *133*, 493.
(12) Yoo, W. C.; Zhang, X. Y.; Tsapatsis, M.; Stein, A. *Microporous Mesoporous Mater.* **2012**, *149*, 147.
(13) Song, W. G.; Marcus, D. M.; Fu, H.; Ehresmann, J. O.; Haw, J. F. *J. Am. Chem. Soc.* **2002**, *124*, 3844.
(14) Wang, Q.; Cui, Z. M.; Cao, C. Y.; Song, W. G. *J. Phys. Chem. C* **2011**, *115*, 24987.
(15) Shin, J.; Camblor, M. A.; Woo, H. C.; Miller, S. R.; Wright, P. A.; Hong, S. B. *Angew. Chem., Int. Ed.* **2009**, *48*, 6647.
(16) Rojas, A.; Arteaga, O.; Kahr, B.; Camblor, M. A. *J. Am. Chem. Soc.* **2013**, *135*, 11975.
(17) Rojas, A.; Martinez-Morales, E.; Zicovich-Wilson, C. M.; Camblor, M. A. *J. Am. Chem. Soc.* **2012**, *134*, 2255.
(18) Rojas, A.; Gomez-Hortiguela, L.; Camblor, M. A. *J. Am. Chem. Soc.* **2012**, *134*, 3845.
(19) Goel, S.; Wu, Z. J.; Zones, S. I.; Iglesia, E. *J. Am. Chem. Soc.* **2012**, *134*, 17688.
(20) Chen, C. Y.; Ouyang, X.; Zones, S. I.; Banach, S. A.; Elomari, S. A.; Davis, T. M.; Ojo, A. F. *Microporous Mesoporous Mater.* **2012**, *164*, 71.
(21) Jackowski, A.; Zones, S. I.; Hwang, S. J.; Burton, A. W. *J. Am. Chem. Soc.* **2009**, *131*, 1092.
(22) Choi, M.; Na, K.; Kim, J.; Sakamoto, Y.; Terasaki, O.; Ryoo, R. *Nature* **2009**, *461*, 246.
(23) Na, K.; Jo, C.; Kim, J.; Cho, K.; Jung, J.; Seo, Y.; Messinger, R. J.; Chmelka, B. F.; Ryoo, R. *Science* **2011**, *333*, 328.
(24) Na, K.; Choi, M.; Park, W.; Sakamoto, Y.; Terasaki, O.; Ryoo, R. *J. Am. Chem. Soc.* **2010**, *132*, 4169.
(25) Jo, C.; Jung, J.; Shin, H. S.; Kim, J.; Ryoo, R. *Angew. Chem., Int. Ed.* **2013**, *52*, 10014.
(26) Wang, Z. P.; Dornath, P.; Chang, C. C.; Chen, H. Y.; Fan, W. *Microporous Mesoporous Mater.* **2013**, *181*, 8.
(27) Moliner, M.; Willhammar, T.; Wan, W.; Gonzalez, J.; Rey, F.; jorda, J. L.; Zou, X. D.; Corma, A. *J. Am. Chem. Soc.* **2012**, *134*, 6473.
(28) Moliner, M.; Gonzalez, J.; Portilla, M. T.; Willhammar, T.; Rey, F.; Liopis, F. J.; Zou, X. D.; Corma, A. *J. Am. Chem. Soc.* **2011**, *133*, 9497.
(29) Lee, J. H.; Park, M. B.; Lee, J. K.; Min, H. K; Song, M. K.; Hong, S. B. *J. Am. Chem. Soc.* **2010**, *132*, 12971.
(30) Xu, R.; Pang, W.; Yu, J.; Huo, Q.; Chen, J. *Chemistry of Zeolite and Related Porous Materials*; Wiley: Singapore, 2007.
(31) Bibby, D. M.; Dale, M. P. *Nature* **1985**, *317*, 157.
(32) Cooper, E. R.; Andrews, C. D.; Wheatley, P. S.; Webb, P. B.; Wormald, P.; Morris, R. E. *Nature* **2004**, *430*, 1012.
(33) Xu, Y.; Tian, Z.; Wang, S.; Hu, Y.; Wang, L.; Wang, B.; Ma, Y.; Hou, L.; Yu, J.; Lin, L. *Angew. Chem., Int. Ed.* **2006**, *45*, 3965.
(34) Parnham, E. R.; Morris, R. E. *J. Am. Chem. Soc.* **2006**, *128*, 2204.
(35) Morris, R. E. *Angew. Chem., Int. Ed.* **2008**, *47*, 442.
(36) Ma, H.; Tian, Z.; Xu, R.; Wang, B.; Wei, Y.; Wang, L.; Xu, Y.; Zhang, W.; Lin, L. *J. Am. Chem. Soc.* **2008**, *130*, 8120.
(37) Cai, R.; Liu, Y.; Gu, S.; Yan, Y. *J. Am. Chem. Soc.* **2010**, *132*, 12776.
(38) Xie, B.; Song, J.; Ren, L.; Ji, Y.; Li, J.; Xiao, F.-S. *Chem. Mater.* **2008**, *20*, 4533.
(39) Xie, B.; Zhang, H.; Yang, C.; Liu, S.; Ren, L.; Meng, X.; Yilmaz, B.; Müller, U.; Xiao, F.-S. *Chem. Commun.* **2011**, *47*, 3945.
(40) Zhang, H.; Yang, C.; Zhu, L.; Meng, X.; Yilmaze, B.; Müller, U.; Feyen, M.; Xiao, F.-S. *Microporous Mesoporous Mater.* **2012**, *155*, 1.
(41) Yang, C.; Ren, L.; Zhang, H.; Zhu, L.; Wang, L.; Meng, X.; Xiao, F.-S. *J. Mater. Chem.* **2012**, *22*, 12238.
(42) Zhang, H.; Xie, B.; Meng, X.; Müller, U.; Yilmaze, B.; Feyen, M.; Maurer, S.; Gies, H.; Tatsumi, T.; Bao, X.; Zhang, W.; De Vos, D.; Xiao, F.-S. *Microporous Mesoporous Mater.* **2013**, *180*, 123.
(43) Wu, Q. M.; Wang, X.; Meng, X. J.; Yang, C. G.; Liu, Y.; Jin, Y. Y.; Yang, Q.; Xiao, F.-S. *Microporous Mesoporous Mater.* **2014**, *186*, 106.
(44) Majano, G.; Delmotte, L.; Valtchev, V.; Mintova, S. *Chem. Mater.* **2009**, *21*, 4184.
(45) Majano, G.; Darwiche, A.; Mintova, S.; Valtchev, V. *Ind. Eng. Chem. Res.* **2009**, *48*, 7084.
(46) Yokoi, T.; Yoshioka, M.; Imai, H.; Tatsumi, T. *Angew. Chem., Int. Ed.* **2009**, *48*, 9884.
(47) Ren, N.; Bronic, J.; Subotic, B.; Lv, X. C.; Yang, Z. J.; Tang, Y. *Microporous Mesoporous Mater.* **2011**, *139*, 197.
(48) Ren, N.; Bronic, J.; Subotic, B.; Song, Y. M.; Lv, X. C.; Tang, Y. *Microporous Mesoporous Mater.* **2012**, *147*, 229.
(49) Kamimura, Y.; Chaikittisilp, W.; Itabashi, K.; Shimojima, A.; Okubo, T. *Chem. Asian J.* **2010**, *5*, 2182.
(50) Kamimura, Y.; Tanahashi, S.; Itabashi, K.; Sugawara, A.; Wakihara, T.; Shimojima, A.; Okubo, T. *J. Phys. Chem. C* **2011**, *115*, 744.
(51) Itabashi, K.; Kamimura, Y.; Iyoki, K.; Shimojima, A.; Okubo, T. *J. Am. Chem. Soc.* **2012**, *134*, 11542.
(52) Kamimura, Y.; Itabashi, K.; Okubo, T. *Microporous Mesoporous Mater.* **2012**, *147*, 149.
(53) Kamimura, Y.; Iyoki, K.; Elangovan, S. P.; Itabashi, K.; Shimojima, A.; Okubo, T. *Microporous Mesoporous Mater.* **2012**, *163*, 282.
(54) Zhang, W.; Wu, Y.; Gu, J.; Zhou, H.; Wang, J. *Mater. Res. Bull.* **2011**, *46*, 1451−1454.
(55) Song, J.; Dai, L.; Ji, Y.; Xiao, F.-S. *Chem. Mater.* **2006**, *18*, 2775.
(56) Wu, Z.; Song, J.; Ji, Y.; Ren, L.; Xiao, F.-S. *Chem. Mater.* **2008**, *20*, 357.
(57) Zhang, L.; Yang, C.; Meng, X.; Xie, B.; Wang, L.; Ren, L.; Ma, S.; Xiao, F.-S. *Chem. Mater.* **2010**, *22*, 3099.
(58) Zhang, H.; Guo, Q.; Ren, L.; Yang, C.; Zhu, L.; Meng, X.; Li, C.; Xiao, F.-S. *J. Mater. Chem.* **2011**, *21*, 9494.
(59) Meng, X.; Xie, B.; Xiao, F.-S. *Chin. J. Catal.* **2009**, *30*, 965.
(60) Li, X.; Xiang, S.; Wu, D.; Liu, Y.; Zhang, X.; Liu, S. *Chem. J. Chin. Univ.* **1981**, *2*, 517.
(61) Warrender, S. J.; Wright, P. A.; Zhou, W. Z; Lightfoot, P.; Camblor, M. A.; Shin, C.-H.; Kim, D. J.; Hong, S. B. *Chem. Mater.* **2005**, *17*, 1272.
(62) Gies, H.; Marler, B.; Therre, J.; Voss H.; Mahker B. W.O. Patent 2,010,037,690, 2010.
(63) Ng, E. P.; Chateigner, D.; Bein, T.; Valtchev, V.; Mintova, S. *Science* **2012**, *335*, 70.
(64) Ng, E. P.; Goupil, J. M.; Vicente, A.; Fernandez, C.; Retoux, R.; Valtchev, V.; Mintova, S. *Chem. Mater.* **2012**, *24*, 4758.
(65) Xu, W. Y.; Dong, J. X.; Li, J. P.; Li, J. Q.; Wu, F. *J. Chem. Soc. Chem. Comm.* **1990**, *10*, 755.
(66) Matsukata, M.; Nishiyama, N. *Microporous Materials* **1996**, *7*, 109.
(67) Deforth, U.; Unger, K. K.; Schüth, F. *Microporous Materials* **1997**, *9*, 287.
(68) Ren, L. M.; Wu, Q. M.; Yang, C. G.; Zhu, L. F.; Li, C. J.; Zhang, P. L.; Zhang, H. Y.; Meng, X. J.; Xiao, F. S. *J. Am. Chem. Soc.* **2012**, *134*, 15173.
(69) Jin, Y. Y.; Sun, Q.; Qi, G. D.; Yang, C. G.; Xu, J.; Chen, F.; Meng, X. J.; Deng, F.; Xiao, F. S. *Angew. Chem., Int. Ed.* **2013**, *52*, 9172.
(70) Morris, R. E.; James, S. L. *Angew. Chem., Int. Ed.* **2013**, *52*, 2163.
(71) Yu, Y.; Xiong, G.; Li, C.; Xiao, F. S. *Microporous Mesoporous Mater.* **2001**, *46*, 23.
(72) Mihailova, B.; Valtchev, V.; Mintova, S.; Faust, A. C.; Petkov, N.; Bein, T. *Phys. Chem. Chem. Phys.* **2005**, *7*, 2756.
(73) Ren, L. M.; Li, C. J.; Fan, F. T.; Guo, Q.; Liang, D. S.; Feng, Z. C.; Li, C.; Li, S. G.; Xiao, F. S. *Chem.—Eur. J.* **2011**, *17*, 6162.